applied sciences

MDPI

Article

Theoretical Analysis on Active Polarization Control of Fiber Laser Based on Root Mean Square Propagation Algorithm

Yifei Shi [1,2,3,4], Yunfeng Qi [2,3,4,*], Hui Shen [2,3,4], Zhao Quan [2,3,4] and Ming Tang [1,*]

[1] School of Optical and Electronic Information, Huazhong University of Science and Technology, Wuhan 430074, China; sh1y1fe13_99@163.com
[2] Aerospace Laser Technology and System Department, Shanghai Institute of Optics and Fine Mechanics, Chinese Academy of Sciences, Shanghai 201800, China
[3] Wang Zhijiang Laser Innovation Center, Shanghai Institute of Optics and Fine Mechanics, Chinese Academy of Sciences, Shanghai 201800, China
[4] Shanghai Key Laboratory of All Solid-State Laser and Applied Techniques, Shanghai Institute of Optics and Fine Mechanics, Chinese Academy of Sciences, Shanghai 201800, China
* Correspondence: dream_7@siom.ac.cn (Y.Q.); tangming@mail.hust.edu.cn (M.T.)

Abstract: High-power linearly polarized fiber lasers are widely used in coherent beam combination, nonlinear frequency conversion, and gravitational wave detection. With the increase in output power, it is challenging for fiber lasers to maintain a high polarization extinction ratio (PER). Combined with intelligent techniques, active polarization control is a prospective method to obtain the laser output with high PER and high stability. We demonstrate a comprehensive model of an active polarization control system. The root mean square propagation (RMS-Prop) algorithm is used to control the non-polarization-maintaining (non-PM) fiber laser to generate linearly polarized laser. The parameters of the RMS-Prop algorithm are theoretically analyzed, including cost function, perturbation amplitude, and global learning rate. The simulation results show that PER is the optimal cost function. When the perturbation amplitude is 0.06 and the global learning rate is 0.6, the system can achieve the optimal control speed and accuracy. By comparison with the stochastic parallel gradient descent (SPGD) algorithm, the RMS-Prop algorithm has an advantage in obtaining higher PER.

Keywords: fiber laser; polarization extinction ratio; active polarization control; root mean square propagation algorithm

check for updates

Citation: Shi, Y.; Qi, Y.; Shen, H.; Quan, Z.; Tang, M. Theoretical Analysis on Active Polarization Control of Fiber Laser Based on Root Mean Square Propagation Algorithm. *Appl. Sci.* **2024**, *14*, 9691. https://doi.org/10.3390/app14219691

Academic Editor: Christos Bouras

Received: 10 September 2024
Revised: 17 October 2024
Accepted: 18 October 2024
Published: 23 October 2024

Copyright: © 2024 by the authors. Licensee MDPI, Basel, Switzerland. This article is an open access article distributed under the terms and conditions of the Creative Commons Attribution (CC BY) license (https://creativecommons.org/licenses/by/4.0/).

1. Introduction

Benefitting from high power, excellent beam quality, and high polarization extinction ratio (PER), high-power linearly polarized fiber lasers have gained extensive attention for their wide applications in industrial manufacturing and scientific research, such as coherent beam combination (CBC) [1–3], nonlinear frequency conversion (NLFC) [4,5], and gravitational wave detection [6]. CBC of high-power linearly polarized fiber lasers is an ideal technology to realize 10 kW-level lasers. In 2020, Müller et al. [3] realized an ultrafast laser delivering 10.4 kW average power based on a CBC system of twelve ytterbium-doped kW-level linearly polarized fiber lasers. NLFC based on high-power linearly polarized fiber lasers in near-infrared band is the primary means of accessing high-power fiber lasers in other bands such as blue–green laser [4] and ultra-violet (UV) laser [5]. The 1 kW linearly polarized single-frequency fiber lasers are considered to be promising laser sources for the next-generation gravitational wave detectors (GWDs), as the sensitivity of GWDs can be increased by increasing the power of laser sources, as well as the degree of polarization [6].

Polarization-maintaining (PM) fibers are usually employed in fiber amplifiers for the generation of linearly polarized fiber lasers. However, compared with non-PM configurations, PM fibers have lower thresholds of nonlinear effects [7] and transverse mode instability (TMI) [8], and in the process of power amplification, the PER of the PM fiber

laser has an overall tendency to deteriorate for thermally induced polarization coupling [9], as a result of which the power scaling of PM fiber amplifiers is more difficult.

Active polarization control of non-PM fiber lasers is an adaptive feedback control scheme combined with intelligent algorithms. The concept of active polarization control was first proposed in optical communication [10], and currently it has been fully developed in both polarization controllers and control algorithms [11,12]. In recent years, the active polarization control of non-PM fiber lasers has shown great potential in high-power linearly polarized fiber lasers. In 2010, Goodno et al. [13] demonstrated a 1.4 kW linearly polarized laser with active polarization control in a non-PM fiber amplifier, and applied it in a CBC system. In 2018, Platonov et al. [14] reported a fiber amplifier with the PER of 16–17 dB and power up to 2.5 kW in non-PM fiber configuration using the active polarization control.

Algorithms are crucial in the active polarization control system, which affect the convergence speed and PER. Various algorithms have been studied in polarization control. In 2008, Li et al. [15] introduced the simulated annealing (SA) algorithm to polarization control, and realized the continuous conversion of the state of polarization (SOP) and the stable SOP output. In 2009, Liu et al. [16] utilized the fast localization algorithm (FLA) as well as the gradient search algorithm to control the polarization efficiently. In 2013, Huang et al. [17] reported a novel algorithm based on FLA to accelerate the control speed and improve the accuracy. In 2020, You et al. [18] proposed a mixed genetic algorithm (GA) and SA algorithm for polarization control, and analyzed the convergence effect theoretically. The above algorithms have not been fully optimized, and show low control bandwidth, low convergence speed, and weak robustness [19]. The stochastic parallel gradient descent (SPGD) algorithm is an optimized gradient descent algorithm with high convergence speed and accuracy, and is preferred in the active polarization control of the high-power fiber laser system. In 2017, Wang et al. [20] and Su et al. [21] realized linearly polarized output power of 1 kW and 1.43 kW by active polarization control based on the SPGD algorithm, with a PER of 14.5 dB and 11.1 dB, respectively. However, the learning rate, or gain factor, of the SPGD algorithm is fixed. It is easy for the algorithm to fall into local optimum when the learning rate is too small, while the convergence is unstable when it is too large.

The root mean square propagation (RMS-Prop) algorithm is an optimized neural network algorithm with an adaptive learning rate, which can be dynamically adjusted and therefore avoids the shortcomings of a fixed learning rate. In the past few years, the RMS-Prop algorithm has been used in the active polarization control system of high-power lasers [22,23]. In 2023, Ren et al. [22] employed an active polarization control technique based on the RMS-Prop algorithm in the narrow linewidth fiber amplifiers and realized a record power of 3.83 kW, with a PER of 12.2 dB. In 2024, utilizing the RMS-Prop algorithm, Wang et al. [23] demonstrated the active polarization control of a high-power linearly polarized ultrafast fiber laser for the first time, with a highest average power of 402.3 W at a repetition rate of 80 MHz and a PER of 11.4 dB. The RMS-Prop algorithm has shown great advantages in the power scaling and the pursuit of a higher PER in high-power fiber lasers. Nevertheless, there exists no report covering the theoretical analysis of polarization control based on the RMS-Prop algorithm.

In this paper, in order to provide an instruction for our further experiments, we theoretically analyzed the control accuracy and convergence speed of the RMS-Prop algorithm in the conversion of a random SOP to the linear polarization, which is reported for the first time. When the PER of output laser is used as the cost function, the amplitude of random perturbation is set to 0.06, and the global learning rate is set to 0.6, the algorithm shows the optimal convergence effect. In comparison with the SPGD algorithm, the RMS-Prop algorithm demonstrated its superiority in the acquisition of a higher PER.

First, in Section 2, the mathematical model of the active polarization control system based on the RMS-Prop algorithm is established. In Section 3, the impact of different parameters on the convergence characteristics of the RMS-Prop algorithm is systematically analyzed. Finally, the performance of the RMS-Prop algorithm is compared with the SPGD algorithm in Section 4.

2. Theoretical Model for Active Polarization Control System

2.1. Mathematical Model of Polarization Controller

In this section, we establish the mathematical model of polarization controller (PC) to calculate the PER of the output laser of an active polarization control system. Figure 1 shows the schematic diagram of active polarization control. The seed source is a phase-modulated single-frequency (SF) linearly polarized fiber laser. The phase modulator (PM) is employed for the suppression of the stimulated Brillouin scattering (SBS) effect, which is one of the key factors that limit the power scaling of fiber lasers. The SF seed laser is phase-modulated through the radio frequency amplified signal, such as sinusoidal signal, white noise signal (WNS), and pseudo-random bit sequence (PRBS) signal, as a result of which the linewidth of the seed laser is broadened and therefore, the threshold of SBS is improved [24,25]. In addition, in the master oscillator power-amplifier (MOPA)-structured fiber laser based on phase-modulated SF seed laser, other nonlinear effects such as self-phase modulation (SPM) and four-wave mixing (FWM) can also be effectively suppressed [24]. After passing through a PC and being amplified by the amplifiers, the laser is finally collimated into free space through the high-power collimator (CO). The output laser is split into two orthogonally polarized beams by a polarization beam splitter (PBS). The S-polarization beam is reflected by the PBS, and the P-polarization beam passes through it and then is sampled by a high-reflectivity mirror M1. A photo detector (PD) is employed to detect the sampled beam of M1 and generates a feedback voltage signal, which will be sent to the algorithm controller, and is processed by RMS-Prop algorithm. By performing the algorithm, the controller generates four-channel voltage signals to PC for controlling the SOP of the seed laser to compensate the effect of polarization noise during amplification process, and finally realize the linearly polarized output laser with high PER.

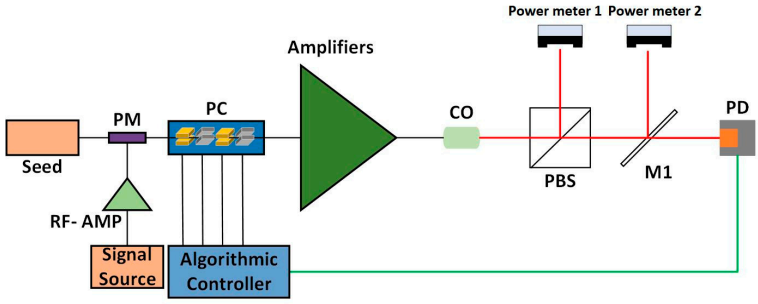


Figure 1. Schematic diagram of active polarization control system of fiber laser: PM, phase modulator; PC, polarization controller; CO: collimator; PBS: polarization beam splitter; PD: photo detector; RF-AMP, radio frequency amplifier.

In the active polarization control system, one type of all-fiber PC, which is composed of four piezoelectric ceramics, is preferred for its fast response and high precision. The fast axis azimuths of four piezoelectric ceramics are fixed. Controlled by the feedback voltage signals, the piezoelectric ceramics squeeze the fiber, and the induced birefringence produces phase retardation in two polarization directions. The retardations of four piezoelectric ceramics vary from 0 to 2π, which is proportional to the applied voltages.

Each piezoelectric ceramic can be described by the Jones matrix [15], as follows:

$$A(\alpha,\delta) = \begin{bmatrix} \cos\alpha & -\sin\alpha \\ \sin\alpha & \cos\alpha \end{bmatrix} \begin{bmatrix} \exp(i\delta/2) & 0 \\ 0 & \exp(-i\delta/2) \end{bmatrix} \begin{bmatrix} \cos\alpha & \sin\alpha \\ -\sin\alpha & \cos\alpha \end{bmatrix}, \quad (1)$$

where α is the azimuth angle of the fast axis and δ is the retardation caused by feedback voltage. Usually, α is 0° for the first and third piezoelectric ceramics, and 45° for the two others.

In fact, adopting three piezoelectric ceramics is enough to realize the control of arbitrary SOP [26], and the fourth one is used to prevent the mutation of SOP during the

endless reset process in the experiments. We neglect the endless reset for the simplification of simulation, and take three piezoelectric ceramics into consideration. The Jones matrix of PC can be given as follows:

$$\begin{array}{l} A(\delta_1,\delta_2,\delta_3) = A_3(0,\delta_3)A_2(\pi/4,\delta_2)A_1(0,\delta_1) \\ = \begin{bmatrix} \cos\frac{\delta_2}{2}\exp\frac{i(\delta_1+\delta_3)}{2} & i\sin\frac{\delta_2}{2}\exp\frac{-i(\delta_1-\delta_3)}{2} \\ i\sin\frac{\delta_2}{2}\exp\frac{i(\delta_1-\delta_3)}{2} & \cos\frac{\delta_2}{2}\exp\frac{-i(\delta_1+\delta_3)}{2} \end{bmatrix} \end{array} \quad (2)$$

Input laser with arbitrary SOP can be expressed as follows:

$$E_{in} = \begin{bmatrix} \cos\theta \\ \sin\theta\exp(i\varphi) \end{bmatrix}, \quad (3)$$

where θ is the azimuth of SOP, and φ is the phase difference in two orthogonal directions. So, the output laser is as follows:

$$\begin{array}{l} E_{out} = A(\delta_1,\delta_2,\delta_3)E_{in} = \begin{bmatrix} E_x \\ E_y \end{bmatrix} = \\ \begin{bmatrix} \exp\frac{i(\delta_1+\delta_3)}{2}\cos\frac{\delta_2}{2}\cos\theta + i\exp\frac{i(2\varphi-\delta_1+\delta_3)}{2}\sin\frac{\delta_2}{2}\sin\theta \\ \exp\frac{i(2\varphi-\delta_1-\delta_3)}{2}\cos\frac{\delta_2}{2}\sin\theta + i\exp\frac{i(\delta_1-\delta_3)}{2}\sin\frac{\delta_2}{2}\cos\theta \end{bmatrix} \end{array} \quad (4)$$

Then, the output laser intensity in horizontal and vertical directions can be given as follows:

$$\begin{array}{l} I_x = E_xE_x^* = \left[\cos\frac{(\delta_1+\delta_3)}{2}\cos\frac{\delta_2}{2}\cos\theta - \sin\frac{(2\varphi-\delta_1+\delta_3)}{2}\sin\frac{\delta_2}{2}\sin\theta\right]^2 + \\ \left[\sin\frac{(\delta_1+\delta_3)}{2}\cos\frac{\delta_2}{2}\cos\theta + \cos\frac{(2\varphi-\delta_1+\delta_3)}{2}\sin\frac{\delta_2}{2}\sin\theta\right]^2 \end{array}, \quad (5)$$

$$\begin{array}{l} I_y = E_yE_y^* = \left[\cos\frac{(2\varphi-\delta_1-\delta_3)}{2}\cos\frac{\delta_2}{2}\sin\theta - \sin\frac{(\delta_1-\delta_3)}{2}\sin\frac{\delta_2}{2}\cos\theta\right]^2 + \\ \left[\sin\frac{(2\varphi-\delta_1-\delta_3)}{2}\cos\frac{\delta_2}{2}\sin\theta + \cos\frac{(\delta_1-\delta_3)}{2}\sin\frac{\delta_2}{2}\cos\theta\right]^2 \end{array} \quad (6)$$

Based on Equations (5) and (6), retardations (δ_1, δ_2, δ_3) determine the laser intensity in two directions, as well as the PER of output laser. In the experiments, we adopt algorithms to control the voltage applied on each piezoelectric ceramic, and thereby optimize their retardations.

2.2. RMS-Prop Algorithm

The RMS-Prop algorithm is the extension of the SPGD algorithm with an adaptive learning rate. The cost function J is a function of the control signals u (u_1, u_2, …, u_N). Random perturbations δu (u_1, u_2, …, u_N) are imposed to u, and thus result in the change in the cost function δJ. According to δu and δJ, the control signal u is updated and iterated until J is optimized to the extreme value.

The steps for the RMS-Prop algorithm can be briefly described as follows:

1. initialize the control signal parameters u = {u_1, u_2, …, u_N }, which is usually randomly given;
2. generate random perturbations with Bernoulli distribution: δu = {δu_1, δu_2, …, δu_N};
3. apply the control signals with positive and negative perturbations: u± = {$u_1 \pm \delta u_1$, $u_2 \pm \delta u_2$, …, $u_N \pm \delta u_N$}, and obtain the cost functions J^+ and J^-;
4. calculate the gradient value, as follows:

$$g = \frac{J^+ - J^-}{J^+ + J^-} \quad (7)$$

5. accumulate the square gradient, as follows:

$$r_{i+1} = \beta r_i + (1-\beta)g^2, \tag{8}$$

where i is the iteration number, the attenuation coefficient β is a hyperparameter, which is set to 0.9, and the initial accumulation of square gradient $r_0 = 0$;

6. update the control signals as follows:

$$u_{i+1} = u_i + \frac{\eta}{\sqrt{r_{i+1}+\varepsilon}} \cdot g \cdot \delta u_i, \tag{9}$$

where η is global learning rate, and the hyperparameter ε is a small constant, which is 0.01 in our simulation;

7. iterate the steps (2)–(6) descripted above until the RMS-Prop controller is turned off.

3. Simulation Results and Discussion

In the simulation, the parameters of the RMS-Prop algorithm including the amplitude of random perturbation δu, global learning rate η, and the cost function J are simulated and optimized to achieve high convergence speed and accuracy.

3.1. Cost Function

There mainly exist three forms of cost functions [18,27], as follows:

$$J_1 = I_y, \tag{10}$$

$$J_2 = \frac{I_y - I_x}{I_y + I_x}, \tag{11}$$

$$J_3 = 10\lg\left(I_y / I_x\right) \tag{12}$$

Among the three cost functions, J_1 is the laser intensity in the y-direction, J_2 is the degree of polarization (DOP), and J_3 is the PER of the output laser. Firstly, the convergence of the RMS-Prop algorithm under different cost functions is simulated. In order that the results are more statistically significant, the program is executed for one thousand times and the calculated data are averaged. When δu = 0.05 and η = 0.4, the simulation results of three cost functions iterating for five hundred times are shown in Figure 2a,b. The horizontal axis in the figure represents the iteration number, and the vertical axes represent DOP and PER, respectively. When J_1 is the cost function, DOP cannot converge to 0.98 within 500 iterations, while it is realized by J_2 and J_3 after 467 and 201 iterations. J_3 has a better convergence performance than the others, which can be seen more obviously from the curve graph of PER. J_3 is chosen as the cost function in our following simulations.

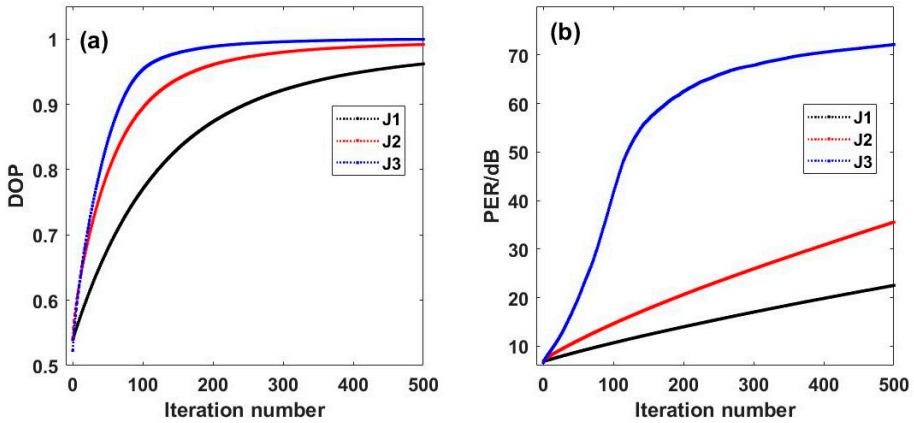


Figure 2. Convergence curves for different cost functions: (**a**) DOP curves; (**b**) PER curves.

3.2. Amplitude of Random Perturbation

The amplitude of random perturbation δu is one of the important parameters for the RMS-Prop algorithm. As δu increases, the convergence speed of the algorithm can be significantly improved. However, when it exceeds a threshold, the convergence will deteriorate, which is not only reflected as instability, but the inability to reach a high convergence value as well.

Figure 3a,b show the convergence curves of the RMS-Prop algorithm with different δu. The cost function is J_3 and η = 0.4. When δu is 0.02 or 0.04, it is too small for the algorithm to converge to 0.99 within 300 iterations. When δu is 0.06, the algorithm converges to a high value at a relatively fast speed. When δu exceeds 0.06, although the algorithm converges extremely fast in the first few steps, the convergence value begins to deteriorate within 300 iterations, which is explicit in the PER curves. Thus, 0.06 is the optimal value for the amplitude of random perturbation, and the algorithm has both a fast convergence speed and high accuracy with δu = 0.06.

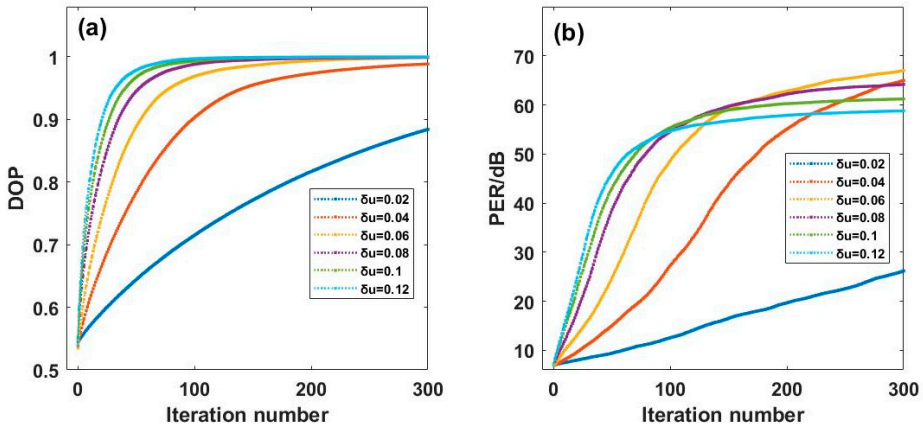


Figure 3. Convergence curves for different perturbation amplitudes: (**a**) DOP curves; (**b**) PER curves.

3.3. Global Learning Rate

Global learning rate η is another important parameter for the RMS-Prop algorithm. The simulated DOP and PER at different global learning rates are shown in Figure 4a,b, with δu = 0.06 and cost function of J_3. The optimal value for the global learning rate is 0.6 according to the curve figures. On the one hand, when η is smaller than 0.6, the convergence speed is relatively slow. On the other hand, when η is larger than 0.6, the convergence of PER degenerates severely, which converges fast in the first few steps while beginning to fluctuate around a relatively small value not long after the algorithm works.

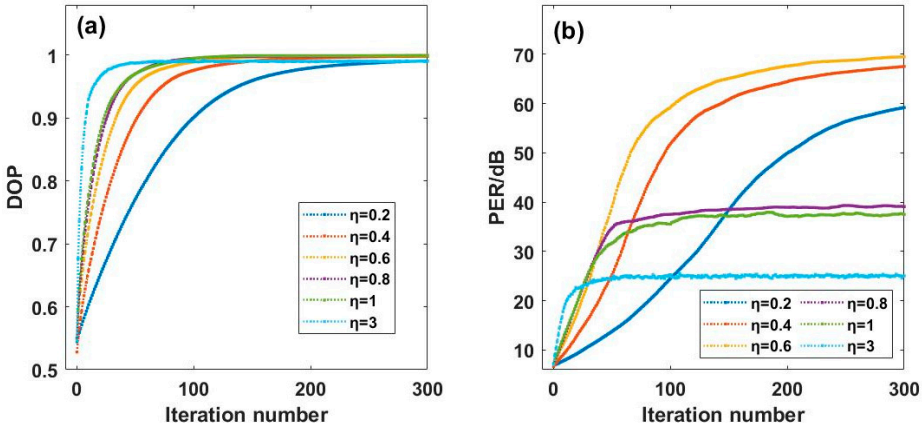


Figure 4. Convergence curves for different global learning rates: (**a**) DOP curves; (**b**) PER curves.

According to the above analysis, the optimal combination of parameters for the RMS-Prop algorithm is concluded. The PER of the output laser is the optimal cost function for the algorithm. When the amplitude of random perturbation is 0.06 and the global learning rate is 0.6, the control effect of polarization is optimal, which means the DOP converges very close to 1 and the PER reaches an extremely high value at a high speed.

4. Comparison with SPGD Algorithm

SPGD is a typical algorithm in polarization control systems, and relevant investigations have been extensively carried out [18–21,27]. In this section, we simulate the convergence performance of the SPGD algorithm for comparison with the RMS-Prop algorithm.

Similar to the RMS-Prop algorithm, the SPGD algorithm is one kind of gradient optimization algorithm, and random perturbations δu with Bernoulli distribution are also imposed to control signals when the SPGD algorithm works. Then, the cost function under positive and negative perturbations, J^+ and J^-, are obtained, respectively. The iteration of control signal u can be expressed as follows:

$$u_{i+1} = u_i + \gamma \delta u_i \left(J^+ - J^- \right) \tag{13}$$

where i is the iteration number, and γ is the gain factor.

Cost function J, perturbation amplitude δu, and gain factor γ are the three main factors that have influence on the convergence performance of the SPGD algorithm. The impact of the three parameters on the algorithm are studied. The simulation results are shown in six sub-pictures (Figure 5a–f). Among them, the three pictures on the left (Figure 5a,c,e) are the results of DOP, and the three pictures on the right (Figure 5b,d,f) are the results of PER. Sub-pictures Figure 5a,b show the convergence performance of the SPGD algorithm with different cost functions. We set δu = 0.05 and γ = 15 according to previous experience of correlational study [18,27]. J_1–J_3 correspond to Formulas (10)–(12). Apparently, J_2 has a better convergence speed and accuracy than J_1, while J_3 fails to converge in the SPGD algorithm. We use J_2 as the cost function in our following simulations. Sub-pictures Figure 5c,d are the simulation results of different perturbation amplitudes. γ is still set to 15, and δu ranges from 0.04 to 0.3. When δu = 0.04, 0.08, and 0.12, DOP converges to 0.95 through 167, 46, and 22 iterations. When δu = 0.16, the convergence value of PER begins to deteriorate. When δu = 0.3, it is clearer from both figures that the convergence value is low and unstable. Sub-pictures Figure 5e,f show the simulation results of different gain factors γ from 10–100. The convergence speed is relatively slow when γ is 10 or 20, converging to 0.99 with 50 and 32 steps, which is less than 20 steps for γ of 40 and 60. When γ is greater than 60, it is difficult for the SPGD algorithm to converge.

When utilizing the DOP of output laser (J_2) as the cost function, and setting the parameter δu to 0.12 and γ to 60, the SPGD algorithm will achieve the optimal convergence effect. We compare the SPGD algorithm with the RMS-Prop algorithm, and their optimal convergence effect of PER is shown in Figure 6. Although the convergence speed of the RMS-Prop algorithm is actually not slow, the SPGD algorithm converges faster obviously. When it comes to convergence accuracy, the RMS-Prop algorithm is superior to that of the SPGD algorithm. When the iteration number reaches a certain value (85 in our simulation), the convergence PER of RMS-Prop algorithm is greater than the SPGD algorithm. After three hundred iterations, the lead is extended to ~10 dB (68.9 dB for the RMS-Prop algorithm and 58.4 dB for the SPGD algorithm. Thus, despite that the RMS-Prop algorithm still has room for improvement in the convergence speed, it is promising to improve the PER of active polarization control system, as well as increasing the power of linearly polarized fiber lasers.

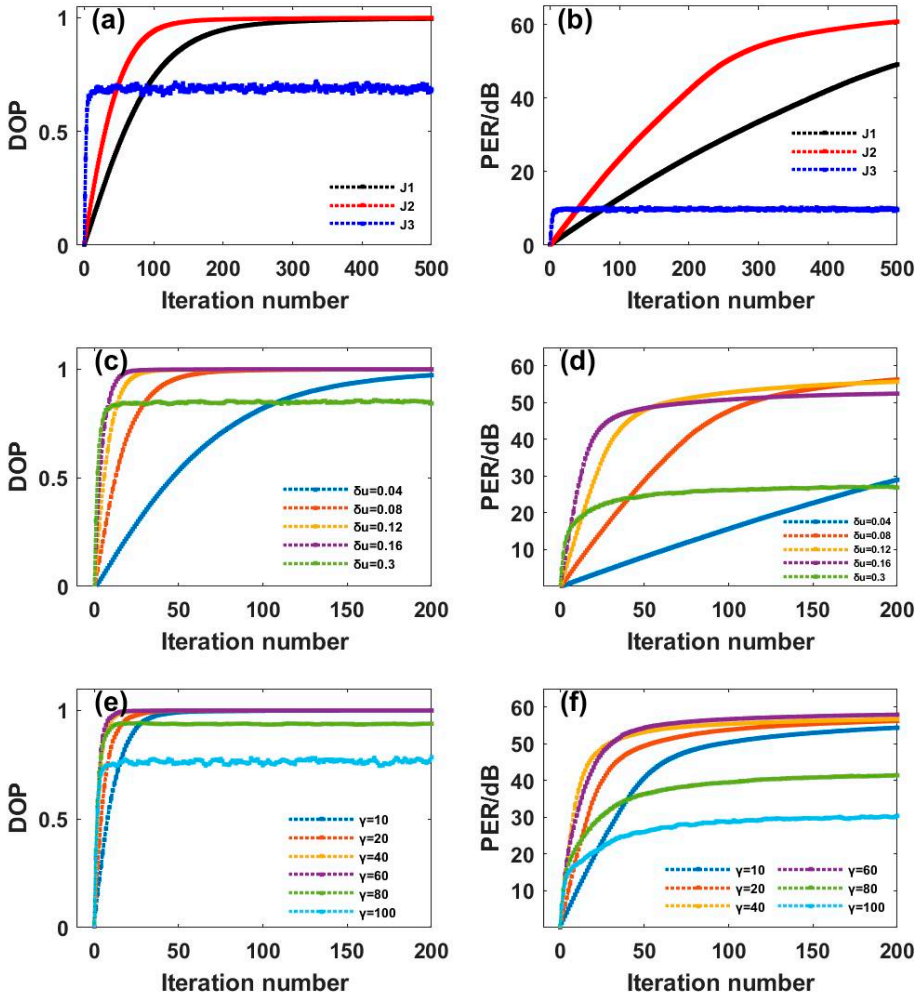


Figure 5. Convergence curves of DOP and PER of SPGD algorithm with different cost functions (**a**,**b**), perturbation amplitudes (**c**,**d**) and global learning rates (**e**,**f**).

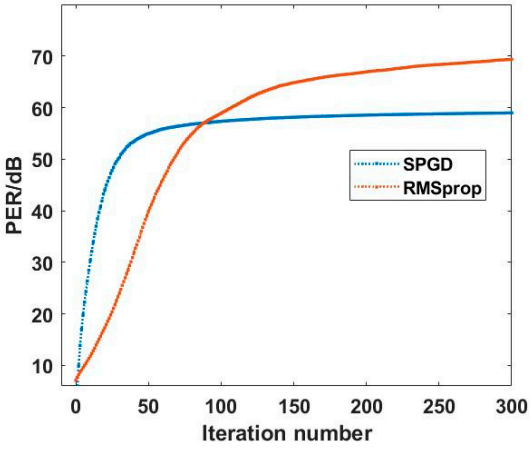


Figure 6. Comparison of RMS-Prop and SPGD algorithms.

5. Conclusions

In summary, we demonstrate an active polarization control model of fiber laser based on the RMS-Prop algorithm, and analyze the impact of different parameters on the convergence effect, including cost function, amplitude of random perturbation, and global learning rate. According to the simulation, when the PER of output laser is utilized as the cost function, the amplitude of random perturbation is set to 0.06, and the global

learning rate is 0.6, the convergence effect of the RMS-Prop algorithm is optimal with high control accuracy and fast convergence speed. In comparison with the SPGD algorithm, the RMS-Prop algorithm is more efficient for pursuing a high PER, which offers a promising method for linearly polarized fiber lasers to obtain higher output power.

Author Contributions: Conceptualization, Y.Q. and H.S.; software, Y.S.; investigation, Y.S.; writing—original draft preparation, Y.S.; writing—review and editing, Y.Q., H.S. and Z.Q.; supervision, Y.Q. and M.T.; project administration, Y.Q. and M.T. All authors have read and agreed to the published version of the manuscript.

Funding: This research was funded by the National Natural Science Foundation of China (NSFC) (62205357).

Institutional Review Board Statement: Not applicable.

Informed Consent Statement: Not applicable.

Data Availability Statement: The original contributions presented in the study are included in the article, further inquiries can be directed to the corresponding author.

Conflicts of Interest: The authors declare no conflicts of interest.

References

1. Liu, Z.; Jin, X.; Su, R.; Ma, P.; Zhou, P. Development Status of High Power Fiber Lasers and Their Coherent Beam Combination. *Sci. China Inf. Sci.* **2019**, *62*, 41301. [CrossRef]
2. McNaught, S.J.; Thielen, P.A.; Adams, L.N.; Ho, J.G.; Johnson, A.M.; Machan, J.P.; Rothenberg, J.E.; Shih, C.-C.; Shimabukuro, D.M.; Wacks, M.P.; et al. Scalable Coherent Combining of Kilowatt Fiber Amplifiers Into a 2.4-kW Beam. *IEEE J. Sel. Top. Quantum Electron.* **2014**, *20*, 174–181. [CrossRef]
3. Müller, M.; Aleshire, C.; Klenke, A.; Haddad, E.; Légaré, F.; Tünnermann, A.; Limpert, J. 10.4 kW Coherently Combined Ultrafast Fiber Laser. *Opt. Lett.* **2020**, *45*, 3083–3086. [CrossRef] [PubMed]
4. Su, M.; You, Y.; Quan, Z.; Shen, H.; Li, Q.; Liu, W.; Qi, Y.; Zhou, J. 321 W High-Efficiency Continuous-Wave Green Laser Produced by Single-Pass Frequency Doubling of Narrow-Linewidth Fiber Laser. *Appl. Opt.* **2021**, *60*, 3836–3841. [CrossRef] [PubMed]
5. Tsubakimoto, K.; Yoshida, H.; Miyanaga, N. 600 W Green and 300 W UV Light Generated from an Eight-Beam, Sub-Nanosecond Fiber Laser System. *Opt. Lett.* **2017**, *42*, 3255–3258. [CrossRef]
6. Steinke, M.; Tünnermann, H.; Kuhn, V.; Theeg, T.; Karow, M.; de Varona, O.; Jahn, P.; Booker, P.; Neumann, J.; Weßels, P.; et al. Single-Frequency Fiber Amplifiers for Next-Generation Gravitational Wave Detectors. *IEEE J. Sel. Top. Quantum Electron.* **2018**, *24*, 1–13. [CrossRef]
7. Stolen, R. Polarization Effects in Fiber Raman and Brillouin Lasers. *IEEE J. Quantum Electron.* **1979**, *15*, 1157–1160. [CrossRef]
8. Brar, K.; Savage-Leuchs, M.; Henrie, J.; Courtney, S.; Dilley, C.; Afzal, R.; Honea, E. Threshold Power and Fiber Degradation Induced Modal Instabilities in High-Power Fiber Amplifiers Based on Large Mode Area Fibers. In *Fiber Lasers XI: Technology, Systems, and Applications*; Proc. SPIE: San Francisco, CA, USA, 2014; p. 89611R. [CrossRef]
9. Wu, Y.; Xiao, Q.; Li, D.; Qi, T.; Tian, J.; Wang, L.; Yan, P.; Gong, M. Thermal Induced Polarization Coupling in Double-Cladding Linearly Polarized Fiber Lasers. *Opt. Commun.* **2022**, *512*, 128036. [CrossRef]
10. Aarts, W.H.J.; Khoe, G.-D. New Endless Polarization Control Method Using Three Fiber Squeezers. *J. Light. Technol.* **1989**, *7*, 1033–1043. [CrossRef]
11. Wang, X.; Zeng, Y.; Liao, R.; Zhao, C.; Tang, M. Reset-Free Adaptive Polarization Controller on a Silicon-Photonic Platform for a Self-Coherent Communication System. *Opt. Lett.* **2023**, *48*, 1546–1549. [CrossRef]
12. Wang, W.; Zhou, Z.; Zeng, Y.; Liu, J.; Yao, G.; Wu, H.; Ding, Y.; Zhou, S.; Yan, S.; Tang, M. CMOS-Compatible High-Speed Endless Automatic Polarization Controller. *APL Photonics* **2024**, *9*, 066116. [CrossRef]
13. Goodno, G.D.; McNaught, S.J.; Rothenberg, J.E.; McComb, T.S.; Thielen, P.A.; Wickham, M.G.; Weber, M.E. Active Phase and Polarization Locking of a 1.4 kW Fiber Amplifier. *Opt. Lett.* **2010**, *35*, 1542–1544. [CrossRef] [PubMed]
14. Platonov, N.; Gapontsev, V.; Yagodkin, R.; De La Cruz, J.; Yusim, A. Up to 2.5-kW on Non-PM Fiber and 2.0-kW Linear Polarized on PM Fiber Narrow Linewidth CW Diffraction-Limited Fiber Amplifiers in All-Fiber Format. In *Fiber Lasers XV: Technology and Systems*; Carter, A.L., Hartl, I., Eds.; SPIE: San Francisco, CA, USA, 2018; p. 13. [CrossRef]
15. Li, W.; Zhang, X.; You, B.; Zou, K.Y. Endless Polarization Control Based on Simulated Annealing Algorithm. In Proceedings of the 2008 IEEE International Symposium on Knowledge Acquisition and Modeling Workshop, Wuhan, China, 21–22 December 2008; IEEE: Wuhan, China, 2008; pp. 275–278. [CrossRef]
16. Liu, Y.; Chi, H.; Zhang, X.; Jin, X.; Zheng, S. A Novel Control Scheme for Four-Plate Retardation Polarization Controller. *Microw. Opt. Technol. Lett.* **2009**, *51*, 124–128. [CrossRef]
17. Huang, Z.; Liu, C.; Li, J.; Zhang, D.; Cheng, H.; Luo, Y.; Hu, Q.; Han, M. Fiber Polarization Control Based on a Fast Locating Algorithm. *Appl. Opt.* **2013**, *52*, 6663–6668. [CrossRef]

18. You, Y.; Qi, Y.; Shen, H.; Zou, X.; He, B.; Zhou, J. Research on Active Polarization Control System of Fiber Laser Based on a Mixed Genetic Algorithm and Simulated Annealing Algorithm. *Acta Opt. Sin.* **2020**, *40*, 2314002. [CrossRef]
19. Jiang, M.; Wu, H.; An, Y.; Hou, T.; Chang, Q.; Huang, L.; Li, J.; Su, R.; Zhou, P. Fiber Laser Development Enabled by Machine Learning: Review and Prospect. *PhotoniX* **2022**, *3*, 16. [CrossRef]
20. Wang, Y.; Feng, Y.; Wang, X.; Yan, H.; Peng, J.; Peng, W.; Sun, Y.; Ma, Y.; Tang, C. 6.5 GHz Linearly Polarized Kilowatt Fiber Amplifier Based on Active Polarization Control. *Appl. Opt.* **2017**, *56*, 2760–2765. [CrossRef] [PubMed]
21. Su, R.; Liu, Y.; Yang, B.; Ma, P.; Wang, X.; Zhou, P.; Xu, X. Active Polarization Control of a 1.43 kW Narrow Linewidth Fiber Amplifier Based on SPGD Algorithm. *J. Opt.* **2017**, *19*, 045802. [CrossRef]
22. Ren, S.; Chang, H.; Ma, P.; Chen, Y.; Wang, G.; Li, W.; Liu, W.; Yao, T.; Zhou, P. 3.38 kW All-Fiberized Narrow Linewidth Fiber Laser Based on Active Polarization Control Using RMS-Prop Algorithm. *Opt. Laser Technol.* **2023**, *166*, 109634. [CrossRef]
23. Wang, T.; Ren, S.; Chang, H.; Ren, B.; Guo, K.; Li, C.; Ma, P.; Leng, J.; Zhou, P. High-Power All-Fiber Linearly Polarized Yb-Doped Chirped Pulse Amplifier Based on Active Polarization Control. *Chin. Opt. Lett.* **2024**, *22*, 041403. [CrossRef]
24. Zheng, Y.; Li, P.; Zhu, Z.; Liu, X.; Wang, J.; Wang, X. Progress in High-Power Narrow-Linewidth Fiber Lasers. *Laser Optoelectron. Prog.* **2018**, *55*, 080002. [CrossRef]
25. Liu, Y.; Lv, Z.; Dong, Y.; Li, Q. Research on Stimulated Brillouin Scattering Suppression Based on Multi-Frequency Phase Modulation. *Chin. Opt. Lett.* **2009**, *7*, 29–31.
26. Zhang, Q.; Zhu, Y.; Su, Y.; Wang, D.; Yang, L. Research on the Polarization Rotation Axis of Variable Retardation Plates Polarization Controller. In Proceedings of the 2012 2nd International Conference on Computer Science and Network Technology, Changchun, China, 29–31 December 2012; IEEE: Changchun, China, 2012; pp. 509–512. [CrossRef]
27. Yin, M.; Su, R.; Wang, X.; Ma, Y.; Ma, P. Theoretical and Experimental Research on Polarization Control of Fiber Laser Based on SPGD Algorithm. *Laser Optoelectron. Prog.* **2018**, *55*, 090602. [CrossRef]

Disclaimer/Publisher's Note: The statements, opinions and data contained in all publications are solely those of the individual author(s) and contributor(s) and not of MDPI and/or the editor(s). MDPI and/or the editor(s) disclaim responsibility for any injury to people or property resulting from any ideas, methods, instructions or products referred to in the content.